

# Superdirectivity-Based Superoscillatory Waveform Design: A Practical Path to Far-Field Sub-Diffraction Imaging

Alex M. H. Wong, Student Member, IEEE,  
George V. Eleftheriades, Fellow, IEEE

The Rogers S. Sr. Department of Electrical and Computer Engineering, University of Toronto, Toronto, Canada.

**Abstract**—Recent interest in superoscillations has led to theoretical investigations as well as proposed applications in imaging and signal processing. In this paper, we elucidate the relationship between superoscillation and the closely related concept of superdirectivity. Key similarities and differences are highlighted, which showcase windows of possibility for practical superoscillatory waveform design. Thereafter, through the example of the Optical Super-Microscope — a far-field super-resolution microscope, we demonstrate how established antenna array theory can be leveraged to design a practical superoscillatory filter, which enables far-field sub-diffraction optical imaging. We end by reporting our current progress with the Optical Super-Microscope and suggest future directions to improve its imaging capability.

**Index Terms**—superoscillation, superdirectivity, sub-diffraction imaging, super-resolution, antenna array.

## I. INTRODUCTION

Superoscillations — a phenomenon whereby, over a finite duration, a waveform oscillates with a faster frequency than its highest constituent frequency components — has recently seen increasing interest and applications. The mathematical groundwork for superoscillatory waves was laid in a series of works in the 1960's by Slepian et al. [1], under the topic of prolate spheroidal wave functions. It was later emphasized by Aharonov et al. [2] and Berry [3], citing its manifestation in quantum physical and optical systems. The field has since undergone theoretical developments, with works which suggest ways to construct superoscillations [3]–[5] and analyze their properties [6]–[8]. In particular, Ferreira and Kempf [4] studied superoscillations in relation to the Nyquist and Shannon limits, and found that while superoscillatory signals oscillate at a faster rate than the Nyquist limit, they still abide by the Shannon limit. They also proved that high energy sidebands must accompany the desired superoscillatory features. The sideband energy (normalized with that of the superoscillatory region) varies polynomially with the apparent spectral width of the superoscillatory features, and exponentially with its duration. By suggesting a need for very high sensitivity, this work and others [9] undermined the practicality of synthesizing superoscillatory waves and using them in imaging systems.

Notwithstanding, sub-wavelength superoscillatory features,

vortices, hotspots and imaging devices have recently been demonstrated [10]–[14]. However, these works and most related works exert very loose control on how the superoscillatory waveform behaves in the non-superoscillatory region — in which most of the waveform's energy must reside [4]. Therefore, while these works demonstrate the feasibility of generating superoscillatory waveforms and verify them in controlled imaging experiments, they leave unanswered the fundamental concern towards the sensitivity of superoscillatory waveforms. An investigation in the direction of sideband control, or better yet, a method for controlling the sidebands of superoscillatory waveforms, should answer this concern from a theoretical standpoint, and produce practical superoscillatory patterns useful for imaging and signal processing.

In the present work, we describe a novel perspective on superoscillations, which enhances our understanding on the phenomenon and provides a useful tool for designing practical superoscillatory waveforms. We achieve this through forming a linkage between superoscillation and superdirectivity — a concept developed some two decades prior to the first mathematical works on superoscillation, but bears much resemblance to the latter. Through this linkage we showcase the design of superoscillatory waveforms and filters by adapting techniques for antenna design. Finally we describe the Optical Super-Microscope, which exemplifies an intriguing imaging application made possible by superdirective antenna inspired superoscillatory filter design.

## II. SUPEROSCILLATION AND SUPERDIRECTIVITY

The essence to the concept of superoscillation is that one can generate sharp oscillations in a waveform despite having limited support in the reciprocal (or Fourier) domain. Fig. 1a-b shows a superposition of five complex exponentials with frequencies less than or equal to 1 Hz, which clearly oscillates faster than 1 Hz across a region of interest (ROI). This exemplifies a temporal superoscillation. Fig. 1c-d shows a similar phenomenon in the spatial domain: several plane waves which have transverse wave numbers  $k_x \leq k_0$  (where  $k_0 = 2\pi/\lambda$  is the wave number of free-space) are superimposed to form a resultant spatial waveform which features a sub-wavelength peak. In this case, superoscillatory wave components widen the

TABLE I  
SUMMARY OF COMPARISON BETWEEN SUPERDIRECTIONALITY AND SPATIAL SUPEROSCILLATION

	Superdirectivity	Spatial Superoscillation
<b>Domain of Limited Extent</b>	$x$	$k_x$
<b>Domain of superoscillation</b>	$k_x$	$x$
<b>Region of Interest (ROI)</b>	Propagating spectrum ( $ k_x  \leq k_0$ )	Designer defined
<b>Sideband Location</b>	Evanescent spectrum ( $ k_x  > k_0$ )	Outside ROI
<b>Far-field mapping</b>	$\theta = \cos^{-1}(k_x/k_0)$ , $\theta \in [0^\circ, 180^\circ]$	N/A
<b>Breaks Diffraction Limit?</b>	Angular	Spatial
<b>Sideband visible?</b>	No	Yes
<b>Physical Effects of Sideband</b>	Increases Q of antenna; Increases sensitivity of antenna; Induces metallic loss.	Take up a portion of waveform energy; Visible sideband may decrease functionality.

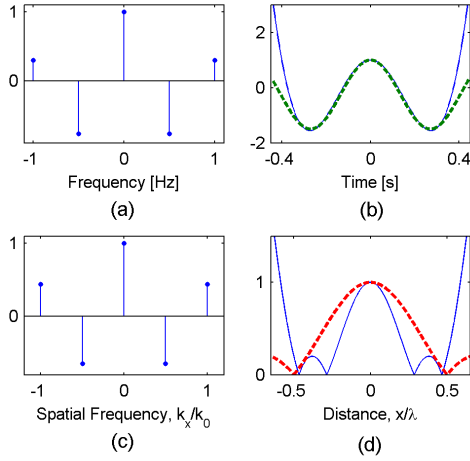


Fig. 1. Examples of superoscillatory waveforms. (a) Spectral weights for five complex exponentials (two sinusoids and a DC offset), with frequencies less than or equal to 1 Hz. (b) The superposition of the complex exponentials displayed in (a), which features a temporary rapid oscillation at 1.85 Hz. The green dashed curve is a 1.85 Hz cosine wave plotted for comparison. (c) The spectral distribution of five plane waves with spatial frequency  $k_x \leq k_0$ . (d) The superposition of plane waves shown in (c), which features a superoscillatory sub-wavelength peak. A diffraction limited sinc (red, dashed) is plotted for comparison.

effective local bandwidth across the ROI, which leads to the formation of a sub-wavelength peak. It is in this manner that superoscillation relates directly to the formation or retrieval of sub-diffraction features using only propagating waves. This stimulates promising application proposals for propagation wave-based far-field sub-diffraction imaging.

Now we consider a superdirective antenna and its antenna pattern, which directly relates to its plane-wave spectrum. To simplify the discussion, we consider an antenna array of  $y$ -directed line sources, which remain invariant in the  $y$ -direction and are isotropic in the  $xz$ -plane. In such a case, the antenna pattern is determined solely by its array factor, or equivalently its line source excitation currents. Fig. 2a shows a diagram of a five-element antenna array, with a total electrical size of 1 m, which is also the wavelength of radiation. Co-ordinates and key geometries are shown in the figure. Fig. 2b shows

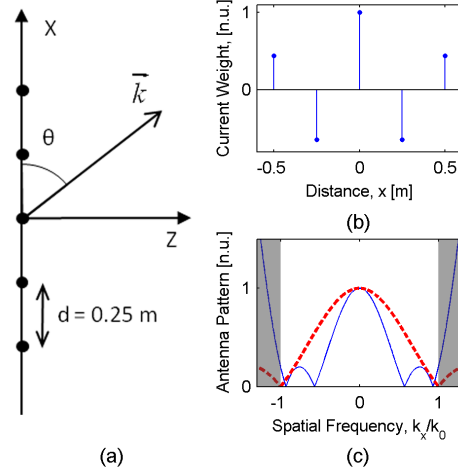


Fig. 2. Examples of a superdirective antenna. (a) A diagram showing the coordinates and geometry for a five element antenna array. (b) Current weights for five isotropic antennas, spaced 0.25 m apart (the wavelength is 1 m). (c) Corresponding spatial frequency profile. The shaded region corresponds to the stored wave region, while the unshaded region corresponds to the superdirective antenna pattern, with  $\theta$  given by (1). The diffraction-limited sinc function for  $NA$  is plotted for comparison (red, dashed).

the current excitation pattern and Fig. 2c shows the antenna pattern for a superdirective antenna, plotted in units of  $k_x$ , which relates to  $\theta$  by

$$\cos(\theta) = \frac{k_x}{k_0}. \quad (1)$$

Clearly, the domain  $\theta \in [0^\circ, 180^\circ]$  maps to  $k_x \in [-k_0, k_0]$ . In this way, the antenna pattern corresponds to the propagation spectrum of the antenna's excitation currents. However, in addition to the propagation spectrum, the plane-wave spectrum also possesses an evanescent spectrum in the region  $|k_x| > k_0$ . These evanescent wave components do not map to a propagation angle, and hence reside in the near-field of the antenna array. Consistent with Fig. 2b-c, it is known that to achieve a sharp angular peak, a superdirective antenna must assume very high near-field, or reactive field components [15]. This corresponds to high energy contents within its evanescent

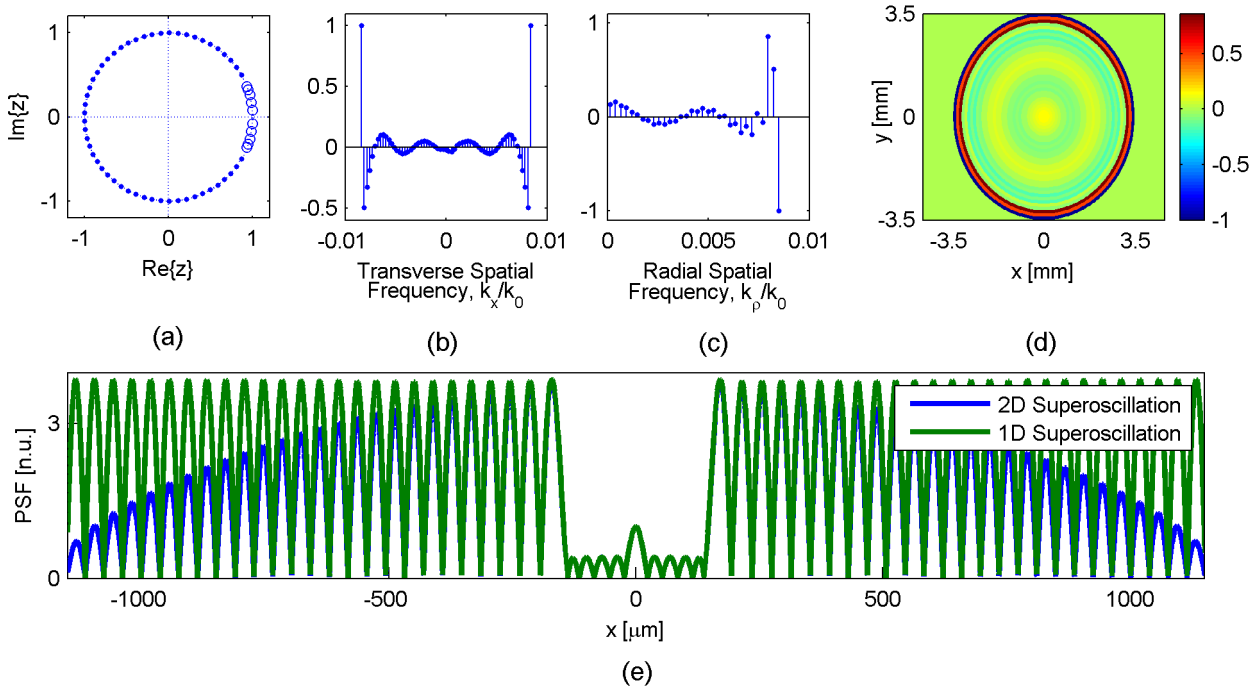


Fig. 3. Design for a Superoscillatory Filter. (a) Locations of zeros corresponding to a 1D superoscillatory waveform. Open circles denote zeros within the ROI; dots denote zeros in the sideband region. (b) The plane-wave spectrum which corresponds to (a). (c) A spectrum of zero-order Bessel functions which superimpose into a 2D waveform having the same null locations on the  $x$ -axis as the 1D superoscillatory waveform. (d) A 2D filter which corresponds to (c). The outer radius of the outermost ring measures approximately 3.5 mm. (e) A plot of the 1D superoscillatory pattern and the  $x$ -cross-section of the 2D counterpart, showing conformity in null locations, pulse width, sidelobe level and sideband amplitude.

spectrum, as shown in the shaded region of Fig. 2c.

Comparing Fig. 2b-c to Fig. 1c-d brings one immediate conclusion: the superdirective antenna pattern in Fig. 2c corresponds to a superoscillatory waveform in the  $k_x$ -domain. This superoscillatory waveform is the Fourier transform of the superdirective current distribution plotted in Fig. 2b; the propagation spectrum of this superoscillatory waveform maps to the antenna pattern through the mapping described by (1). This relationship is true in general for all superdirective antennas.

Table 1 lists a comparison between a superdirective plane-wave spectrum and a spatial superoscillatory waveform, which can be summarized as follows. The excitation current distribution to a superdirective antenna has a plane-wave spectrum which superoscillates in the  $k_x$ -domain. The extent of the current distribution is limited by the antenna size in the  $x$ -domain. In the  $k_x$ -domain its ROI is the propagating spectrum. A  $k_x$ -domain superoscillation can result in a narrow antenna beam, which breaks the angular diffraction limit [16]–[18], just as the spatial superoscillation can result in a narrow peak which breaks the spatial diffraction limit [17], [18]. A key distinction between the two phenomenon is the fact that superdirectivity involves a far-field mapping, whereby free-space diffraction filters out the evanescent spectrum, and renders the sideband invisible from the antenna pattern. This is not the case for spatial superoscillations. High energy sidebands are inseparable from the superoscillatory waveform,

and render the waveform sensitive in the following sense: plane wave components of a spatial superoscillatory waveform must delicately interfere and the signal noise level must be low for superoscillatory features to be faithfully reproduced, which are generally of low amplitude compared to the sideband. This sense of waveform sensitivity is very different than that for a superdirective antenna, where the high-energy evanescent spectrum physically manifests itself as a strong reactive near-field, which dissipates due to metallic loss, and hence undermines the efficiency (and hence gain) of the superdirective antenna. This difference makes it possible to reduce the sensitivity requirement of a spatial superoscillatory waveform (or filter), and hence lead to practical implementations of superoscillation-based imaging devices.

### III. THE OPTICAL SUPER-MICROSCOPE

As an illustrative example, we describe our work in constructing the Optical Super-Microscope (OSM) — a far-field super-resolution optical microscope [19]. Leveraging the relation between superdirectivity and superoscillations, we apply Schelkunoff superdirective antenna design to obtain a set of “excitation currents”. We then implement these excitation currents as a modulation in the transverse  $k$ -domain. This modulation results in a superoscillatory impulse response (or point spread function) in the spatial domain, suitable for sub-diffraction imaging applications.

Fig. 3 shows a design procedure for the superoscillatory filter. Fig. 3a shows the location of zeros on the  $z$ -plane. Circles denote 12 zeros placed within the ROI, while dots denote 50 zeros placed outside the ROI. While in superdirective antenna design, zeros are seldom placed outside the visible region (equivalent to the ROI), the technique of zero placement antenna design does not restrict the designer from placing zeros in the invisible region. In designing superoscillatory waveforms, the placement of zeros outside the ROI allows some degree of control on sideband behaviour, while a higher concentration of zeros within the ROI enables superoscillation therein [20]. The zero locations in Fig. 3a correspond to the plane-wave spectrum in Fig. 3b and the 1D superoscillation waveform in Fig. 3e. To extend the waveform into a 2D equivalent, a 2D modulation in the transverse  $k$ -domain is designed with a superposition of zero order Bessel functions, such that the radial nulls of the superimposed waveform coincide with the  $x$ -domain nulls of its 1D counterpart. Fig. 3c shows the resulting Bessel function distribution, Fig. 3d shows the corresponding 2D filter, while Fig. 3e plots a cross-section of the 2D waveform on the  $x$ -axis alongside the 1D superoscillatory waveform. The comparison in Fig. 3e shows the preservation of key waveform specifications such as the superoscillatory beamwidth, the extent of the ROI, sidelobe ripples within the ROI, and the sideband amplitude. This signifies the successful design of a 2D superoscillation waveform.

The spectral weights, as displayed in Fig. 3d, are implemented on a spatial light modulator (SLM), the LCD panel size for which is as depicted in Fig. 3d. Two Fourier Transforming (FT) lens sandwich the SLM to perform forward and inverse Fourier transforms, such that the 2D superoscillation waveform, shown in Fig. 3e, becomes the impulse response (or point spread function) of the imaging system. The focal length of the FT lenses (400 mm) forms the working distance of the OSM; the half width of the SLM (3.5 mm) forms the effective aperture of the OSM. Dividing the latter by the former gives a numerical aperture of  $NA = 0.00864$ , which for HeNe laser illumination ( $\lambda = 632.8$  nm) corresponds to an Abbé diffraction limit of

$$d = \frac{\lambda}{2NA} = 36.7 \mu\text{m}. \quad (2)$$

While at present the numerical aperture is admittedly small, proof-of-principle experiments have demonstrated the OSM's capability to perform far-field sub-diffraction imaging.

Fig. 4 shows our experimental results with the OSM. Fig. 4a shows an experimental image of a small hole  $10 \mu\text{m}$  in diameter. We observe that the superoscillatory sidebands are separated from the sub-diffraction peak by a  $150 \mu\text{m}$  distance. This separation corresponds to the ROI of the superoscillatory waveform design process. A circle of half that radius forms the field of view (FOV) of the OSM: whenever objects are located within the FOV, they can be faithfully imaged without spurious interference with the high-intensity sideband. The sideband intensity, clamped down by placement of zeros into the non-

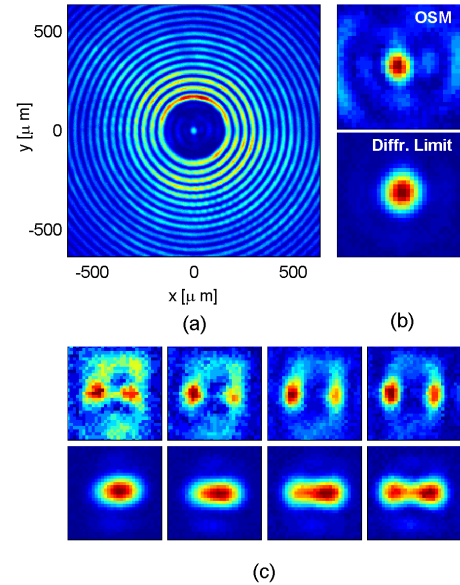


Fig. 4. Experimental results for the OSM. (a) Experimentally measured PSF of the OSM, featuring an isolated sub-diffraction peak in the ROI, and high-intensity rings outside the ROI. (b) A close up on the sub-diffraction peak (top panel), compared to the diffraction-limited peak (bottom panel). (c) A series of close up images showing successful two-aperture resolution by the OSM (top row). The same two apertures are not resolved by a diffraction-limited imaging system with the same  $NA$  (bottom row). The apertures are  $15 \mu\text{m}$  in diameter. The edge-to-edge separations of the apertures, from left to right, are  $30 \mu\text{m}$ ,  $35 \mu\text{m}$ ,  $40 \mu\text{m}$  and  $45 \mu\text{m}$  respectively. [19]

superoscillatory region, is about four times that of the central peak. This does not pose serious problems with waveform sensitivity. Fig. 4b shows a close up of the experimentally measured central peak. This peak is clearly sharpened in comparison to the diffraction-limited PSF — obtained by replacing the superoscillatory filter with a uniform aperture of the same size.

Fig. 4c shows results from a two-point characterization experiment, which demonstrates the OSM's ability to resolve two closely-spaced circular apertures, which cannot be resolved by a diffraction-limited system. When the two apertures are horizontally separated by varying set of distances (increasing from left to right), the top row shows successful resolution by the OSM, while the bottom row shows, for the most part, unsuccessful resolution by the diffraction-limited system. From results from both the one-point and two-point characterization experiments, the demonstrated OSM improves the minimal resolvable lengths to about 70% of the diffraction-limit. Our current research directions aim to improve the quality of the superoscillatory filter, the extent of the FOV and the  $NA$  of the OSM, in effort to develop the OSM into a practical tool for far-field sub-wavelength optical imaging.

#### IV. CONCLUSION

In this paper we examined the close relationship between the concepts of superoscillation and superdirectivity. Upon concluding that superdirectivity is a case of generating super-

oscillatory waveforms in the transverse  $k$ -domain, we leveraged superdirective antenna design techniques to help design superoscillatory waveforms in the spatial domain which are practical for implementation in sub-diffraction imaging devices. As one example, we described our progress in building an Optical Super-Microscope, which uses a superoscillatory filter to achieve far-field sub-diffraction optical imaging. Our current proof-of-principle prototype achieves sub-diffraction imaging with a minimum resolvable distance 70% that of the diffraction limit. We also commented on current directions towards developing the OSM for sub-wavelength far-field imaging.

## REFERENCES

- [1] D. Slepian and H. O. Pollak, "Prolate spheroidal wave functions, fourier analysis and uncertainty i," *Bell System Technical Journal*, pp. 43–63, 1961.
- [2] Y. Aharonov, J. Anandan, S. Popescu, and L. Vaidman, "Superpositions of time evolutions of a quantum system and a quantum time-translation machine," *Physical Review Letters*, vol. 64, no. 25, pp. 2965–2968, Jun 1990.
- [3] M. V. Berry, *Faster than Fourier*, ser. Quantum coherence and reality: in celebration of the 60th Birthday of Yakir Aharonov. Singapore: World Scientific, 1994, pp. 55–65.
- [4] P. J. S. G. Ferreira and A. Kempf, "Superoscillations: faster than the nyquist rate," *IEEE Transactions on Signal Processing*, vol. 54, no. 10, pp. 3732–3740, Oct 2006.
- [5] P. J. S. G. Ferreira, A. Kempf, and M. J. C. S. Reis, "Construction of aharonov-berry's superoscillations," *Journal of Physics A : Mathematical and General*, vol. 40, no. 19, pp. 5141–5147, May 2007.
- [6] A. Kempf, "Black holes, bandwidth and beethoven," *Journal of Mathematical Physics*, vol. 41, pp. 2360–2374, Apr 2000.
- [7] M. Calder and A. Kempf, "Analysis of superoscillatory wave functions," *Journal of Mathematical Physics*, vol. 46, no. 1, p. 012101, Jan 2005.
- [8] E. Katzav and M. Zchwartz, "Yield-optimized superoscillations," *IEEE Transactions on Signal Processing*, vol. 61, no. 12, pp. 3113–3118, Jun 2013.
- [9] H. J. Hyvärinen, S. Rehman, J. Tervo, J. Turunen, and C. J. R. Sheppard, "Limitations of superoscillation filters in microscopy applications," *Opt. Lett.*, vol. 37, no. 5, pp. 903–905, Mar 2012. [Online]. Available: <http://ol.osa.org/abstract.cfm?URI=ol-37-5-903>
- [10] F. M. Huang, N. Zheludev, Y. Chen, and F. J. G. De Abajo, "Focusing of light by a nanohole array," *Applied Physics Letters*, vol. 90, no. 9, p. 091119, Feb 2007.
- [11] M. R. Dennis, A. C. Hamilton, and J. Courtial, "Superoscillation in speckle patterns," *Optics Letters*, vol. 33, no. 24, pp. 2976–2978, Dec 2008.
- [12] T. Brunet and J. L. Thomas, "Transverse shift of helical beams and subdiffraction imaging," *Physical Review Letters*, vol. 105, no. 3, p. 034301, Jul 2010.
- [13] S. Kosmeier, M. Mazilu, J. Baumgartl, and K. Dholakia, "Enhanced two-point resolution using optical eigenmode optimized pupil functions," *Journal of Optics*, vol. 13, p. 105707, Sept. 2011.
- [14] E. T. F. Rogers, J. Lindberg, T. Roy, S. Savo, J. E. Chad, M. R. Dennis, and N. I. Zheludev, "A super-oscillatory lens optical microscope for subwavelength imaging," *Nature Materials*, vol. 11, pp. 432–435, 2012.
- [15] N. Yaru, "A note on super-gain antenna arrays," *Proceedings of the IRE*, vol. 39, no. 9, pp. 1081–1085, Sep 1951.
- [16] S. A. Schelkunoff, "A mathematical theory of linear arrays," *Bell System Technical Journal*, vol. 22, pp. 80–107, Jan 1943.
- [17] A. M. H. Wong and G. V. Eleftheriades, "Adaptation of schelkunoff's superdirective antenna theory for the realization of superoscillatory antenna arrays," *IEEE Antennas and Wireless Propagation Letters*, vol. 9, pp. 315–318, Apr 2010.
- [18] —, "Sub-wavelength focusing at the multi-wavelength range using superoscillations: an experimental demonstration," *IEEE Transactions on Antennas and Propagation*, vol. 59, no. 12, pp. 4766–4776, Dec 2011.
- [19] —, "An optical super-microscope for far-field, real-time imaging beyond the diffraction limit," *Scientific Reports*, vol. 3, p. 1715, 2013.
- [20] —, "Temporal pulse compression beyond the fourier transform limit," *IEEE Transactions on Microwave Theory and Techniques*, vol. 59, no. 9, pp. 2173–2179, Sep 2011.